An assessment of the wind influence in local inertial 1D hydrodynamic flow routing

Fernando Mainardi Fan[1], Vitória Ache Rocha Lopes[1]
[1]Universidade Federal do Rio Grande do Sul, Instituto de Pesquisas Hidráulicas

ABSTRACT

One-dimensional (1D) hydrodynamic modeling studies generally do not take into account the influence of wind, although literature experiences demonstrate the importance of this information in some cases. In this context, the present work had the objective to investigate this matter further, studying the influence of wind on hydrodynamic 1D modeling results and proposing an abacus for the rapid verification of the possible maximum influence of a wind on a simulation. In order to carry out the work we propose a modified version of the inertial flow routing method including the wind shear stress. Several tests were performed to assess model stability and to understand further the wind influence on river flow conditions. As a result, an equation and an abacus were proposed to estimate maximum percentage depth variations that can be caused by continuous wind influence under different characteristics of river flow and wind action. Results also showed that it is possible to obtain a stable solution with the addition of the wind shear stress, but time interval values should be carefully selected considering high disturbances due to wind influence.

Keywords: *Hydrodynamic Modelling, Wind Shear, Local Inertial Method*

INTRODUCTION

Flood routing algorithms are used as part of hydrodynamic models or hydrological models to simulate processes such as floods and droughts, to assess land use and climate change effects in water resources, to develop flood forecasting systems, to simulate water quality variations, among many other applications. These algorithms can be developed considering one, two or three spatial dimensions. One-dimension (1D) is usually considered when simulating rivers (CHOW, 1988).

Usually hydrological and hydrodynamic models, despite allowing for the simulation of complex hydrodynamic systems, do not account for the wind influence. Even though the wind can exert substantial effect over such systems. A good example of this importance can be found in the work of Mashriqui et al. (2014), who proposed a flood forecasting tool for the river Potomac, a wide river located near the cost of United States and hence very susceptible to wind influence. The authors concluded that only the use of the HEC-RAS hydrodynamic model (USACE, 2010), which considers the full Saint-Venant Equations, wouldn't be sufficient to predict water levels in the river due to the non-consideration of wind influence. Additionally, the authors advise that the inclusion of wind shear in the HEC-RAS model would aid to improve flood forecasting systems for 14 coastal rivers in EUA.

In another study, Rámon et al. (2016) analyzed, among other factors, wind influence in mixing in the confluence of two large rivers in Spain and concluded that this influence, depending on wind direction and velocity, can employ important modifications in the system.

Other wind effects relevance studies are reported in literature, and particularly in systems comprehending a river connected to an estuary, as (ESCOBAR et al., 2004; GONG et al., 2009; D'AQUINO et al., 2011; BACOPOULOS et al., 2012).

Indeed the wind influence plays an important role in the dynamics of large water bodies such as lakes and lagoons (Ji, 2008). Therefore, most 2D and 3D hydrodynamic models usually applied to simulate these systems include this effect, such as the models MIKE (DHI, 2011), IPH-A (BORCHE, 1996), Delft-3D (DELTARES, 2014), IPH-ECO (Fragoso et al., 2009) and POM (BLUMBERG; MELLOR, 1987). But, despite the experiences showing that the account of wind effects in 1D hydrodynamic models can be beneficial, it is not a common practice.

Considering the exposed, the present study aimed to further investigate the possibility of including the wind shear effects in a 1D hydrodynamic flow routing method, and to better understand how the wind would affect one dimensional river simulations.

To accomplish with these objectives, the present study was conducted considering two stages, as follows:

- Stage 1: Simulation of different scenarios of hypothetical river reaches to verify stability and better understand wind influence in the equations;
- Stage 2: Proposition of an equation and an abacus to calculate maximum variations of water level due to continuous wind stress.

The hydrodynamic flow routing method tested in the present study was the local inertial method, based in a simplification of the Saint-Venant Equations. As far as we

concern, this method has never been previously applied in the literature considering wind friction terms.

The full Saint-Venant Equations are known to describe one-dimensional non-permanent flow and are vastly applied (CUNGE et al., 1980; CHANSON, 2004). However, considering that hydrological models are used to simulate all or most of the processes that occur in hydrological systems, simpler flow routing methods than the full Saint-Venant Equations are commonly used (HODGES, 2013). These methods include, for example, the Muskingum-Cunge method (CUNGE, 1969; Collischonn et al., 2007), the Muskingum method (McCARTHY, 1938; NEITSCH et al., 2002; HATTERMANN et al., 2005) and linear reservoir methods (NGO-DUC et al., 2007; DECHARME et al., 2008). Due to simplifications. these methods do not allow for the simulation of floodplain storage and backwater effects.

The local inertial method, also called only "inertial", proposed by Bates et al. (2010), poses as a promising alternative to the simple methods used in hydrological models (Fan et al., 2014). The algorithm only excludes the advective inertial term of the Saint-Venant dynamic equation and, therefore, allows for the simulation of storage in floodplains and backwater effects. The authors Fan et al. (2014) and Montero et al. (2013), for example, verified similar results when applying the inertial method and the full Saint-Venant equations for one-dimension simulations.

Motivated by the good performance of inertial equations testing's, Pontes et al. (2015, 2017) proposed a modified version of the MGB-IPH hydrological model (Collischonn et al., 2007) using the inertial flood routing algorithm and applied the model successfully in the Araguaia River basin, which comprehends very large floodplain areas. This version of the model was also applied by Lopes (2015, 2017), who simulated basins and lagoon systems obtaining satisfactory results of water levels inside the lagoons. Lopes (2015, 2017) concluded that the combination of the inertial routing and storage simulations inside the lagoon, even considering only one-dimension, were satisfactory to estimate water levels and inundated areas in the complex hydrodynamic and hydrological system of the Patos Lagoon basin (southern Brazil).

The inertial flow routing method is also the basis of hydrodynamic models such as LISFLOOD-PF (BATES et al., 2010) and Cama-Flood (YAMAZAKI et al., 2013). The latter was applied in a global scale and compared to the previous version of the model, which was based on the non-inertial equations. The authors concluded that, considering explicit numerical approximations, the inertial method required larger time intervals than the non-inertial method, resulting in more stable and efficient simulations.

The next section of this paper presents the theoretical arrangement of the study. Further sections present the two stages tests, results, discussions and conclusions.

WIND STRESS IN THE LOCAL INERTIAL FLOW ROUTING ALGORITHM

The inertial flow routing algorithm is based on a simplification of the Saint-Venant equations that neglects only the advective inertial terms of the dynamic equation (BATES et al., 2010). The resulting formulation is presented by equations 1 (Continuity) and 2 (Dynamic):

$$\frac{\partial A}{\partial t} + \frac{\partial Q}{\partial x} = 0 \quad (1)$$

$$\frac{\partial Q}{\partial t} + g.A\frac{\partial h}{\partial x} - g.A.S_o + g.A.S_f = 0 \quad (2)$$

in which A represents the cross-sectional area (m^2), Q represents water flow (m^3/s), x is the longitudinal distance (m), t is the time (s), So is the bottom slope (m/m), h is the river depth (m), Sf is the friction slope (m/m) and g is the gravitational acceleration (m/s^2). The first term of Equation 2 represents de conservation of momentum and the remaining terms represent external forces that act in the flow: pressure, gravitational and frictional resistance, respectively.

The wind stress is a tangential force that acts on the water surface and can be written as (Ji, 2008):

$$\tau = \rho_{air}.C_d.U^2 \quad (3)$$

in which ρ_{air} is the air density (kg/m^3), Cd is the wind stress coefficient (dimensionless) and U is the wind velocity in the direction of the flow (m/s).

To add the wind stress force to the dynamic equation of the inertial method some modifications have to be made to Equation 3: (i) Considering that the wind stress acts in the water surface and that the longitudinal distance in the differential dynamic equation (Equation 2) is infinitesimal, the equation 3 should be multiplied by the width of the river reach; (ii) The density of air should be divided by the water density as Equation 2 was previously divided by this term in its formulation; (iii) The wind velocity should be considered as a vector and maintain the wind direction. This can be done by multiplying the wind velocity by its absolute value. The resulting dynamic equation is Equation 4:

$$\frac{\partial Q}{\partial t} + g.A\frac{\partial h}{\partial x} - g.A.S_o + g.A.S_f - B.C_D.|U|.U = 0 \quad (4)$$

in which the relative density of air was combined to the wind stress coefficient in the parameter C_D (dimensionless) here called wind friction coefficient. B is the river width (m). Positive wind velocities favor the flow and negative values

of U act against flow direction.

Assuming a rectangular channel, that Sf can be estimated using the Manning equation, and using the explicit finite differences numerical approximation proposed by Bates et al. (2010), progressive in time and centered in space, Equation 4 can be written as:

$$Q_{i+\frac{1}{2}}^{k+1} = \frac{\left(\left(Q_{i+\frac{1}{2}}^{k}\right) - g.B.\Delta t.\left(h_{i+\frac{1}{2}}^{k}\right)\frac{\left(y_{i+1}^{k} - y_{i}^{k}\right)}{\Delta x} + \Delta t.B.C_D.|U|.U\right)}{\left(1 + \frac{g.\Delta t.\left(\left|q_{i+\frac{1}{2}}^{k}\right|\right).n^2}{B\left(h_{i+\frac{1}{2}}^{k}\right)^{7/3}}\right)} \quad (5)$$

in which i refers to space, k refers to time, Δt is the time interval, Δx is the length of the river section, and y represents the water level. The position i + ½ represents the end of the section i, the position i - ½ represents the beginning of the section I, and i represents the center of the section, for example, $Q_{i+\frac{1}{2}}^{k+1}$ is the flow in the end of the section i in time interval k+1, y_{i+1}^{k} represents the water level in the center of section i +1 and in the kth time interval. $h_{i+\frac{1}{2}}^{k}$ refers to the depth located between sections i and i+1 in the kth time interval, calculated by Equation 6.

$$h_{i+\frac{1}{2}}^{k} = max\left[y_i^k; y_{i+1}^k\right] - max[z_i; z_{i+1}] \quad (6)$$

where z_{i+1} is the bottom level of the river section i +1. Using the same numerical scheme, Equation 1 can be written:

$$h_i^{k+1} = h_i^k - \frac{\Delta t}{B.\Delta x}\left(Q_{i+\frac{1}{2}}^{k+1} - Q_{i-\frac{1}{2}}^{k+1}\right) \quad (7)$$

In the method algorithm, equations 6, 5 and 7 are applied sequentially, first by knowing as an initial condition the water levels and flows in all sections in the first time interval. First equation 6 is applied to calculate $h_{i+\frac{1}{2}}^{k}$ in all sections in time interval k, then Equation 5 in applied to calculate de flow in all sections in time interval k+1 and finally Equation 7 is applied to calculate the water depth in all sections in time k+1; which allows for the calculation of water level knowing the values of z in all sections.

Because the algorithm was derived using an explicit numerical method, there is the need to respect the Courant-Friedrichs-Levy condition. Therefore, the definition of the time interval must satisfy Equation 8:

$$\Delta t = \alpha \frac{\Delta x}{\sqrt{gh}} \quad (8)$$

in which α is a coefficient equal to or lower than 1. Values lower than 0.9 are advised (Bates et al.,2010; Yamazaki et al., 2013).

STAGE 1: SIMULATION EXPERIMENTS

A hypothetical river reach was considered in this study. The definition of its characteristics was based on the lower Jacuí River (RS, Brazil) in the reach between the confluence with Taquari River (RS, Brazil) and the Guaíba Lake (RS. Brazil). This reach is very likely to be influenced by wind due to being in a flat area, having a large width, and being upstream to a large lake, which motivated its selection.

The reach has very low bed slope, assumed 1 cm/km. The average width is approximately 800 m and the average flow is approximately 1000 m³/s. The Manning coefficient of 0.03 was adopted and a C_D value of $1x10^{-6}$ was selected for the tests. The original reach has approximately 50 km of length, however a 100km length was considered in the hypothetical reach to avoid the influence of boundary conditions on the flow. The upstream boundary condition used is a constant inflow and the downstream boundary condition assumed is a normal depth. The hypothetical reach and other parameters are resumed on Table 1.

Table 1. General reach characteristics and simulation parameters.

Characteristics	Value
Length	100 km
Simulation duration	500 h
Δx	2 km
α	0.7
B	1000 m³/s
S	800 m
n	0.01 m/km
C_D	$1x10^{-6}$

Two different wind profiles were assessed: (i) a constant wind profile, considering constant and continuous wind action; and (ii) a pulse wind profile, considering a pulse of wind with a 30h duration. The profiles are displayed on Figure 1. In both profiles, the wind starts to act after 30 hours.

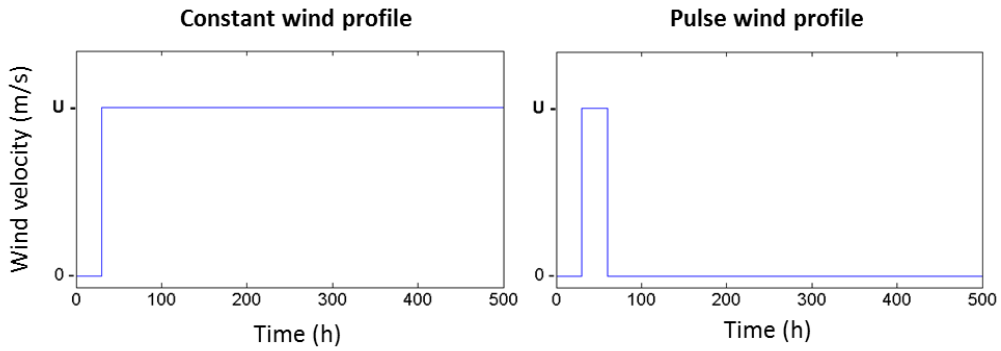

Figure 1: Wind action profiles.

Seven simulations were performed:

1. Simulation of the hypothetical river reach considering the constant wind influence (constant profile) testing wind velocities and directions;
2. Simulation of the hypothetical river reach considering the 30h pulse of wind (pulse profile) testing wind velocities and directions;
3. Simulation considering one extreme wind velocity and direction scenario (-15 m/s, against flow direction) for pulse and constant profiles, testing reach lengths to verify influence of boundary conditions;
4. Simulation of the hypothetical river reach testing low and high flow conditions considering the constant wind profile with -10 m/s wind velocity (against the flow);
5. Simulation testing different values of bed slope using the constant wind profile with -10 m/s wind velocity against the flow;
6. Simulation testing different values of reach width using the constant wind profile with -10 m/s wind velocity against the flow;
7. Simulation testing different values of wind friction coefficient using the constant wind profile with -10 m/s wind velocity against the flow;

In all simulations figures of flow and water depth variation with time are presented displaying five equally spaced river sections (from the first section, displayed in blue, to the last section, displayed in red). For scenarios 1 and 2, curves of water depth transversal profiles are presented displaying 10 time intervals (from the first time interval, displayed in blue, to a selected interval based on results, called upper limit time interval (U.L), displayed in red).

Simulation 1 – Influence of a constant wind profile

This simulation intended to verify the influence of constant wind action on the flow characteristics considering six different wind velocities: -5 m/s, -10 m/s, -15 m/s, 5 m/s, 10 m/s and 15 m/s. Results are displayed on figures 2 to 4. On Figure 4, the upper limit (U.L.) time interval of the plotted curves was 300 h.

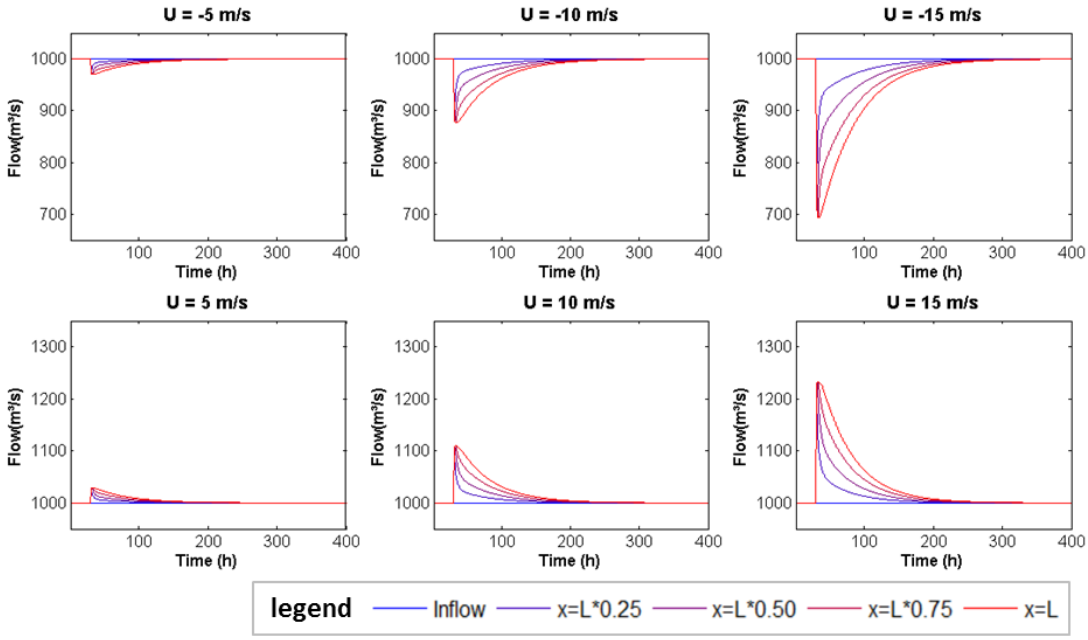

Figure 1 – Flow hydrographs under continuous wind influence.

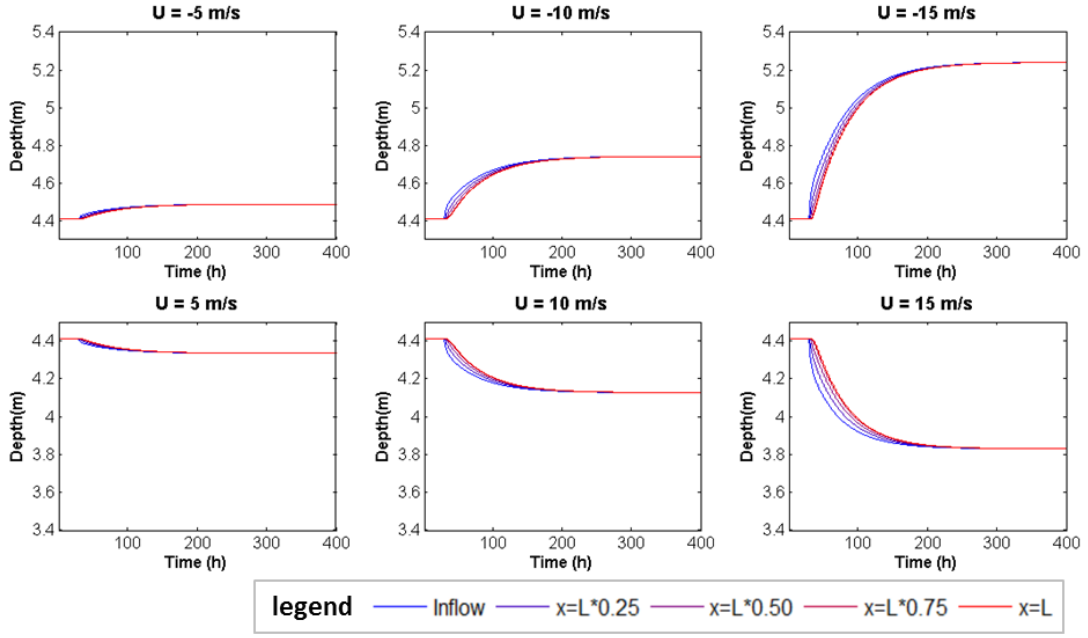

Figure 2 – Water depth versus time under continuous wind influence.

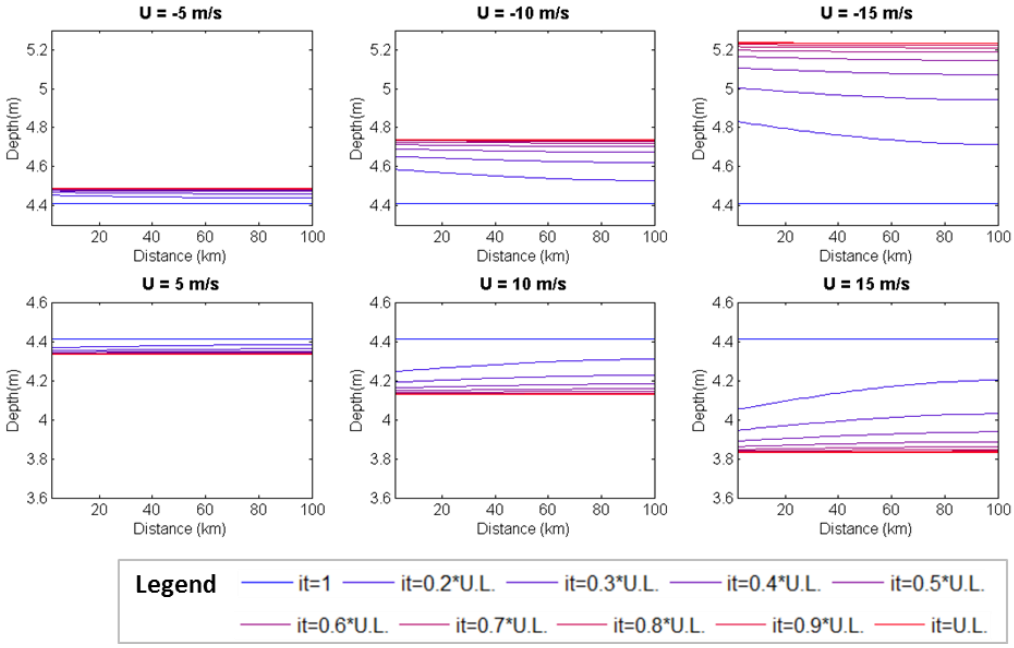

Figure 3 – Water depth longitudinal profiles under continuous wind influence

Figure 2 shows that once wind starts acting there is an immediate disturbance in flow which reaches its maximum flow variation not long after wind started. Considering negative (positive) wind velocities, the variation is negative (positive) with an associated decrease (increase) in flow. Also, the greater the wind velocity is, the greater is the flow variation, e.g. for a wind velocity of -15m/s the flow in the last section can reach approximately 700 m³/s, while considering a wind velocity of -10 m/s, the flow in the last section has a maximum decrease to only approximately 870 m³/s. In addition, absolute variations are greater for negative wind velocities, e. g. the maximum flow variation in the last section associated to a wind with -15 m/s is 300 m³/s, approximately 60 m³/s greater than the variation correspondent to 15 m/s.

After the maximum flow variation is reached soon after the wind started, it begins to decrease progressively until the flow returns to the previous value of 1000 m³/s. The time that the system takes to return to permanent condition also depends on wind velocity magnitude, which means that the greater the disturbance in the system the more time the system takes to return to permanent conditions.

The behavior of the flow is connected to the behavior of water depth, which can be seen in Figure 3. As soon as the wind starts acting, the water depth starts varying with maximum rate, this rate progressively decreases until it reaches zero and the water depth reaches a new permanent value. This occurs in the same time as the flow returns to the previous value of 1000 m³/s. It can therefore be concluded that under continuous and constant wind action, after enough time, the system converges to a new steady state balance condition with the same flow and a different water depth. The wind action can facilitate water flow with positive velocities causing a decrease in depth, and can dam the water flow with negative velocities causing an increase in depth. As occurs in the flow behavior, the greater the wind velocity is, the greater is the disturbance in water depth, which is also greater for negative velocities.

Figure 4 shows the longitudinal profiles in different time intervals. In the earlier time intervals, after wind action starts, curved profiles are formed with greater (smaller) depths upstream and smaller (greater) depths downstream for negative (positive) wind velocities. As time passes the differences of depth in the profile diminish until there are no differences in different sections in the new steady state balance.

Simulation 2 – Influence of a wind pulse

This simulation intended to verify the influence of continuous and constant wind action on the flow characteristics considering 6 different wind velocities: -5 m/s, -10 m/s, -15 m/s, 5 m/s, 10 m/s and 15 m/s. Results are shown in figures 5 to 7. On Figure 7 the upper limit time interval of the plotted curves was 300 h.

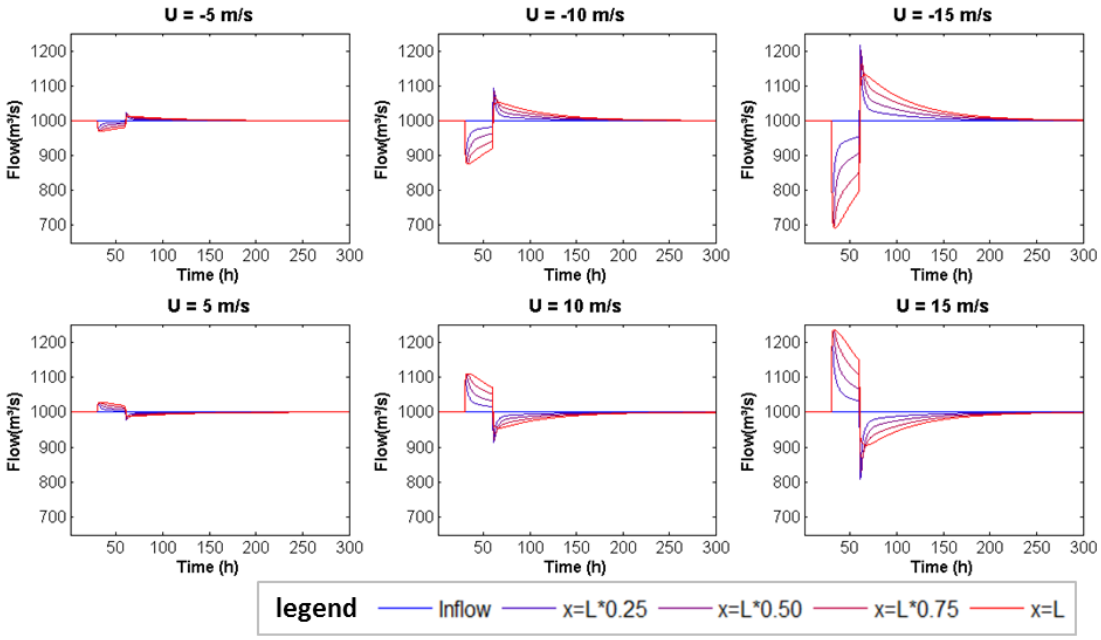

Figure 4 - Flow hydrographs under the pulse wind profile influence

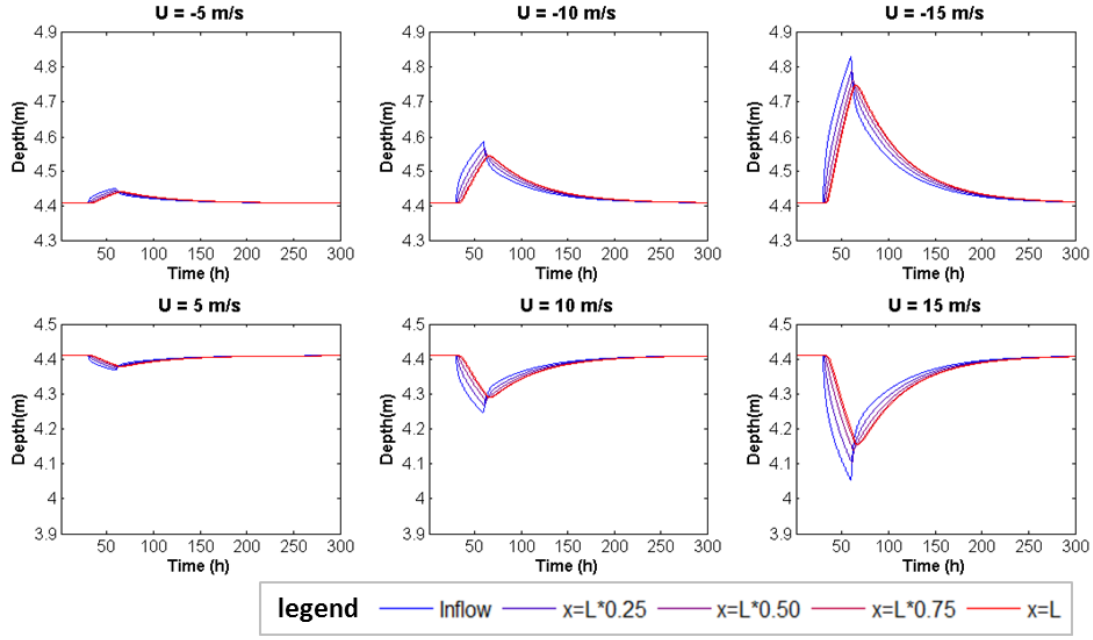

Figure 5 - Water depth versus time under the pulse wind profile influence

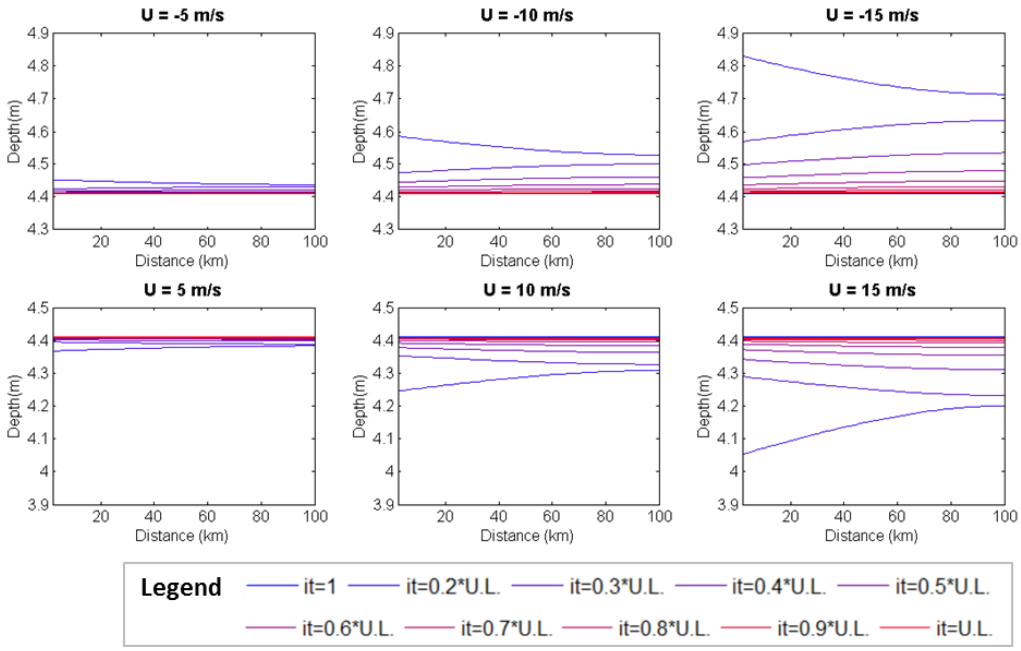

Figure 6 - Water depth longitudinal profiles under the pulse wind profile influence

Until 60 hours of simulation, figures 5, 6 and 7 show the same behavior as figures 2, 3 and 4. Considering negative wind velocities, while the wind acts, the flow is lower than the normal flow and the water depth increases, creating a curved longitudinal profile with greater water depths upstream. When the wind stops, all the water that was piled up ought to leave the system to re-establish the previous permanent equilibrium, which causes an immediate increase in flow to greater values than the normal flow condition. Additionally, just after the wind stops, a wave is created by the difference of water level and propagates downstream. After that, the profile changes, with smaller depths upstream and greater depths downstream. As the time passes the differences between upstream and downstream water levels diminishes as well as the value of mean water level. This happens until there are no differences of water depth in the longitudinal profile and the depth reach the previous condition. The contrary occurs considering positive velocities.

Another distinguish effect can be noted on Figure 6, the dislocation of water level peaks (positive or negative), which happen before in upstream sessions. In addition, downstream, the peeks are less sharp and with lesser magnitude than upstream.

Simulation 3 – Influence of reach length

This simulation was performed with the objective to verify the influence of the hypothetical reach length on the flow response to wind action (-15 m/s) and on the influence of the upstream boundary condition. The lengths of 25 km, 50 km and 100 km were compared considering both continuous and pulse wind profiles. Results are displayed in figures 8 and 9, considering a continuous wind profile, and in figures 10 and 11, considering a pulse wind profile.

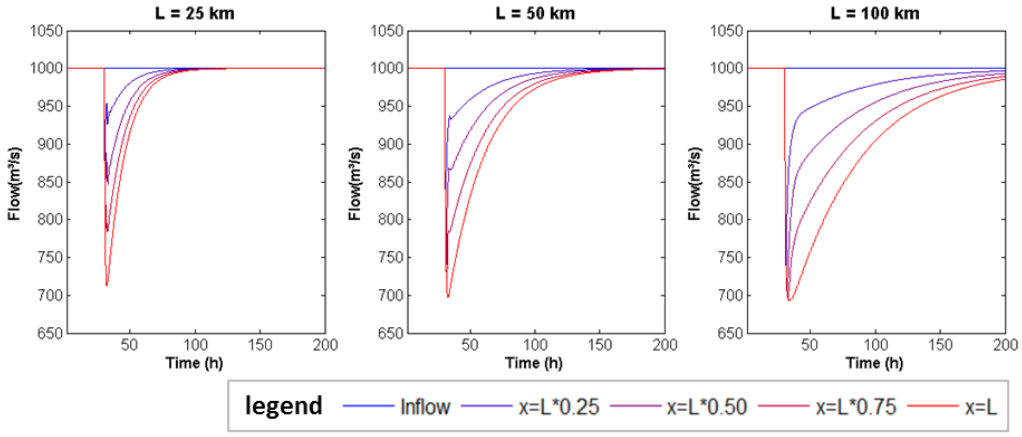

Figure 7 - Flow hydrographs under continuous wind influence for different reach lengths and U=-15 m/s.

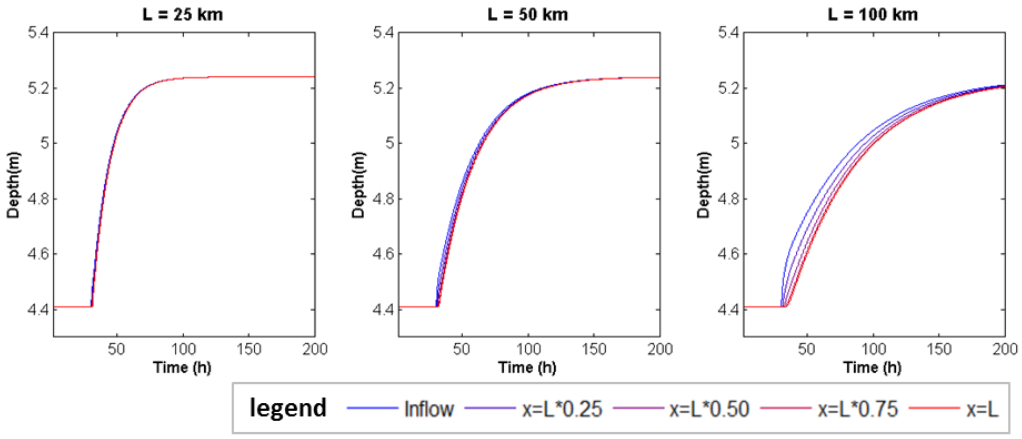

Figure 8 – Water depth versus time under continuous wind influence for different reach lengths and U=-15 m/s.

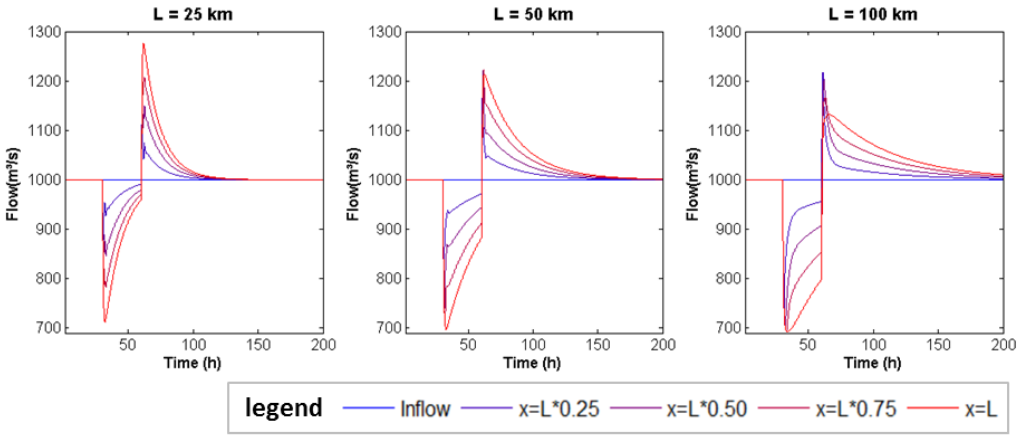

Figure 9 – Flow hydrographs under the pulse wind profile influence for different reach lengths and U=-15 m/s.

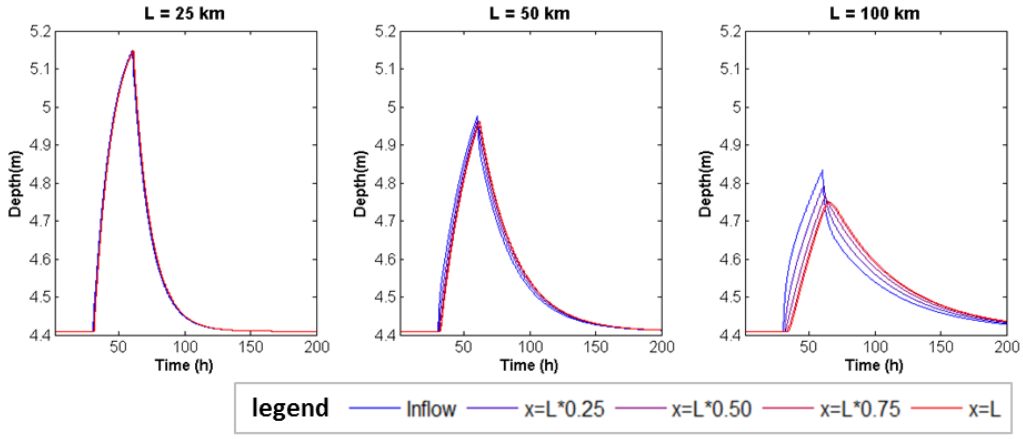

Figure 10 – Water depth versus time under the pulse wind profile influence for different reach lengths and U=-15 m/s.

Analyzing figures 8 and 9 one can verify that small oscillations in flow occur considering shorter reach lengths. This can be explained by the reflection of flow variations on the boundary conditions, which propagate downstream and upstream until they are dissipated. The correspondent water depth variations are too small to be seen on the figures.

The longer the reach is, the longer it takes for a new equilibrium condition to be stablished. E.g. for a 25 km reach, after the wind starts blowing, it takes approximately 70 h for the system to reach equilibrium, for 50 km, the period is approximately 140 h and for 100 km it takes 220 h. This is related to the fact that there is more water in the system to pile up for longer reaches, because continuous wind action changes de water storage in the system and the water storage absolute variation due to continuous wind action is greater for longer reaches.

From figures 10 and 11 one can notice that in response to the longer times required by longer reaches to reach equilibrium under continuous wind influence, the time for the system to return to previous conditions under the pulse profile is also longer. Hence, when considering wind influence over large systems, there has to be noted that this influence may last much longer than the wind action period due to the inertia of the system.

Considering longer reaches, flow hydrographs and water depth variations with time are smother and take larger periods to propagate downstream.

Simulation 4 – Influence of inflows

This simulation was performed to assess the influence of continuous wind (-10 m/s) in the flow considering different inflow values. The inflows values of 100 m³/s, 1000 m³/s and 5000 m³/s were selected to correspond to low flow, average flow, and high flow periods usually observed in the Jacuí River. Results are presented in figures 12 and 13.

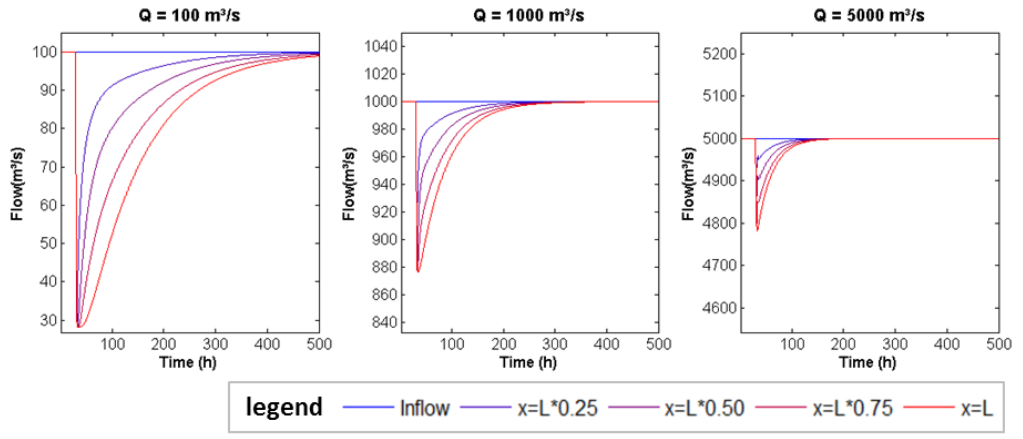

Figure 11 - Flow hydrographs under continuous wind influence for different inflow values and U=-10 m/s.

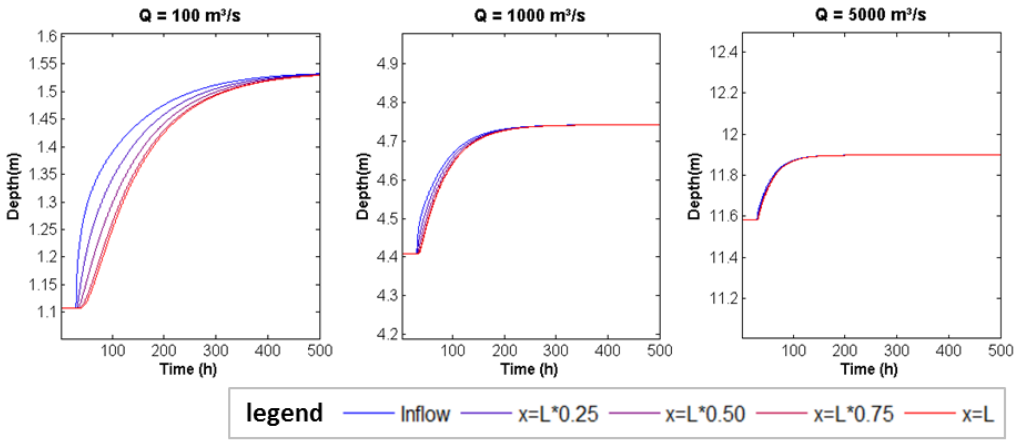

Figure 12 - Water depth versus time under continuous wind influence for different inflow values and U=-10 m/s.

The results presented on Figure 12 show that the absolute variation of flow is greater for higher inflow conditions, however the associated relative variation considerably is lower. E.g. for an inflow of 100 m³/s the maximum flow variation is approximately 70 m³/s which corresponds to a decrease of 70%. Considering an inflow of 5000 m³/s, the variation is approximately 200 m³/s representing a decrease of flow of only 4%.

The influence of boundary conditions, manifested through small flow oscillations in early periods after wind incidence started, can be perceived for the inflow value of 5000 m³/s. This is probably related to the higher water velocity under this condition which makes the variations of flow, although relatively smaller, to propagate more rapidly (i.e. with greater celerity). This can be attested by the decrease of these oscillations using larger reach widths. E.g. Considering the same conditions but a river width of 2000 m, although resulting in larger flow disturbance due to wind action, these flow oscillations do not occur.

Figure 13 shows that for lower inflow periods the wind exerts more influence on the water depth, especially if related to previous conditions. For example, considering an inflow of 100 m³/s, the depth variation reaches 40 cm which corresponds to an increase of depth of approximately 36%; considering 5000 m³/s of inflow this variation is approximately 30 cm and corresponds to an increase of depth of only 2.6%.

Once more, greater disturbance in flow conditions due to wind stress is related to longer periods to reach the new state of equilibrium.

Simulation 5 – Influence of bed slope

Simulation 5 was performed to assess the influence of bed slope on flow characteristics under continuous wind stress (-10 m/s). The values of 50 m/km, 5 m/km, 0.5 m/km, $5x10^{-2}$ m/km, $5x10^{-3}$ m/km e $5x10^{-4}$ m/km were tested. These values were selected to comprehend very steep and very flat scenarios. For this simulation a smaller value of α (0.01) was necessary to simulate steep slopes with no numerical instability. Results are displayed in figures 14 and 15.

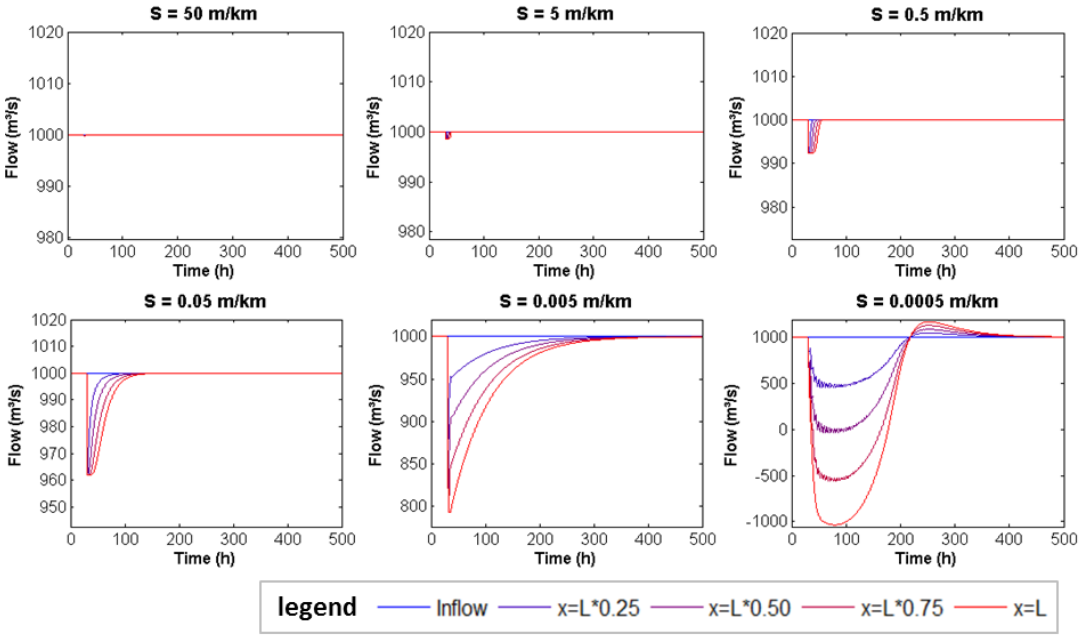

Figure 13 - Flow hydrographs under continuous wind influence for different bed slope (S) values and U=-10 m/s.

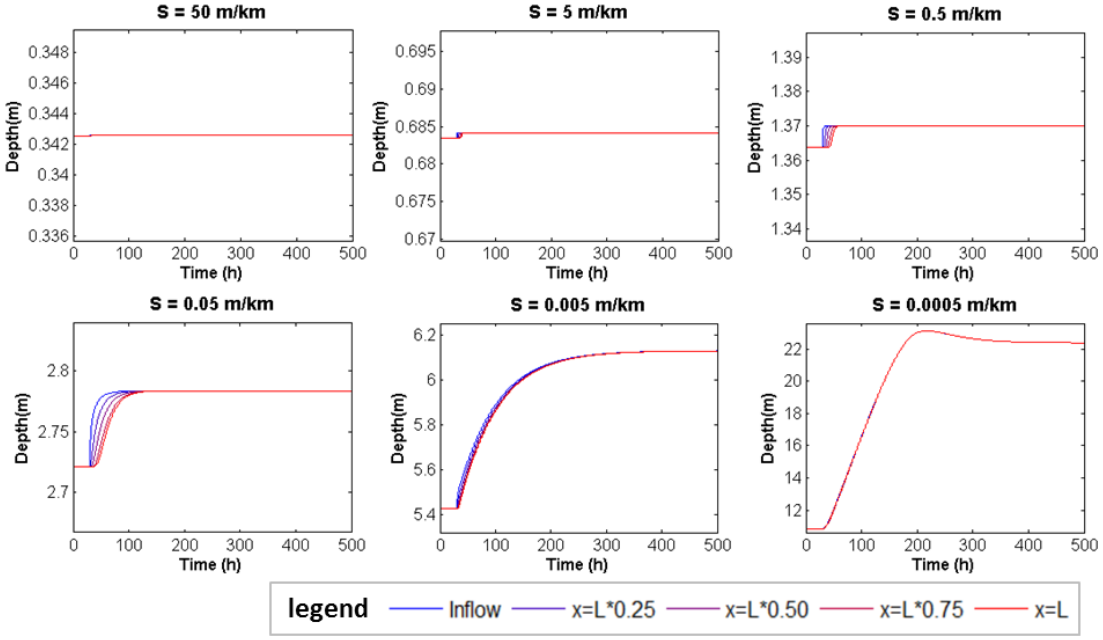

Figure 14 – Water depth versus time Flow under continuous wind influence for different bed slope (S) values and U=-10 m/s.

From the analysis of figures 14 and 15 it can be noted that wind effect is greater for lower bed slope configurations. Considering bed slope values equal or greater than 0.5 m/km, the variations in depth are not significant. Considering the slope of 0.05 m/km, the variation is only 6 cm, which corresponds to an increase of approximately 2% of water depth and a decrease of approximately 4% of flow.

Considering a slope of $5x10^{-3}$ m/km, the increase in depth is much greater, achieving an absolute variation of approximately 70 cm and an increase of 13%. The decrease of flow in this case was approximately 20%. Small oscillations were apparent in the flow hydrograph, which are not only related to the flow celerity, but especially to the magnitude of the disturbance caused by the wind action. These oscillations do not occur with a wind velocity of -5 m/s.

Considering the slope of $5x10^{-4}$ m/km, which is an unmeasurable flat slope very difficult to be found in riverine natural environments, a particular behavior can be noticed. Under this hypothetical extremely flat condition, the wind shows a major influence in flow characteristics. The water depth increases 120% in the new equilibrium and the flow reaches negative values decreasing over 200%. The influence of the wind is strong enough to cause an increase in depth greater than the increase associated to the new equilibrium, which causes a flow wave to propagate with associated increase in flow to greater values than the inflow. Many oscillations occur in this case due to the susceptibility of the system to wind influence. These are also potentialized by the establishment of negative flows that compete with the positive inflows. Oscillations considering these characteristics still occur even for very small wind velocities. This is probably related to the very small bottom slope which allows oscillations to propagate in both directions with low dissipation of their energy.

Simulation 6 – Influence of river width

This simulation was performed to assess the influence of river width under constant wind stress (-10 m/s). The widths of 100 m, 500 m, 1000 m, 2000 m, 4000 m and 8000 m were tested to comprehend a wide variety of scenarios. Results are displayed in figures 16 and 17.

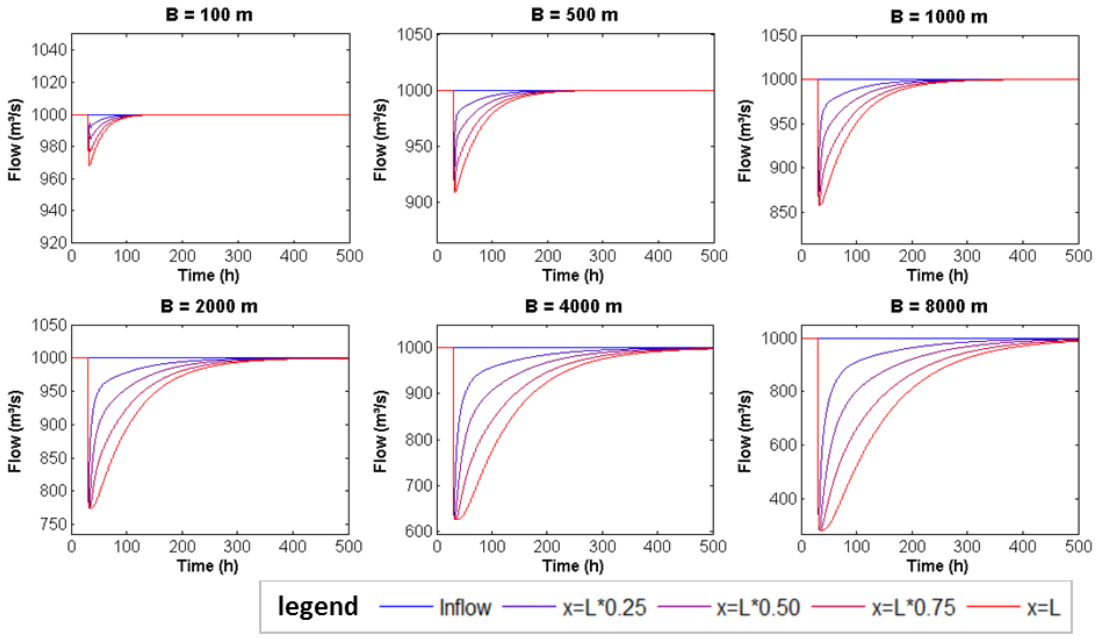

Figure 15 - Flow hydrographs under continuous wind influence for different reach width (B) values and U=-10 m/s.

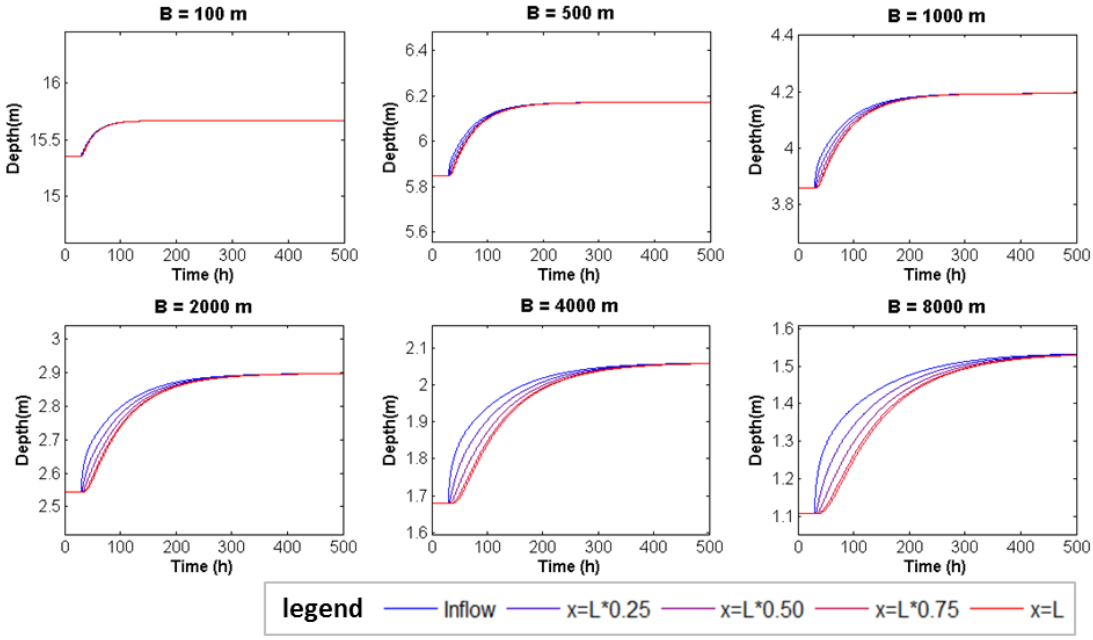

Figure 16 - Water depth versus time Flow under continuous wind influence for different reach width (B) values and U=-10 m/s.

Through the analysis of figures 16 and 17, it was observed that simulations considering larger widths result in greater variations of flow conditions due to wind effect. E. g. considering a width value of 100 m, the water depth variation is 30 cm corresponding to an increase of 2%; for the value of width of 8000 m the variation reaches approximately 42 cm, corresponding to an increase of 40 %. Small oscillations can be noticed for the width of 100 m, due to the effect of the greater celerity of this scenario.

Simulation 7 – Influence of the wind friction coefficient

The objective of simulation 7 was to assess the influence of the wind friction coefficient under constant wind stress (-10 m/s). The coefficients of 0.5×10^{-6}, 1.0×10^{-6}, 1.5×10^{-6}, 2.0×10^{-6}, 3.0×10^{-6}, 4.0×10^{-6}, were tested to comprehend a wide variety of scenarios. Values as large as 4.0×10^{-6} were reported in literature (PAZ *et al.*, 2005; WU, 1982).

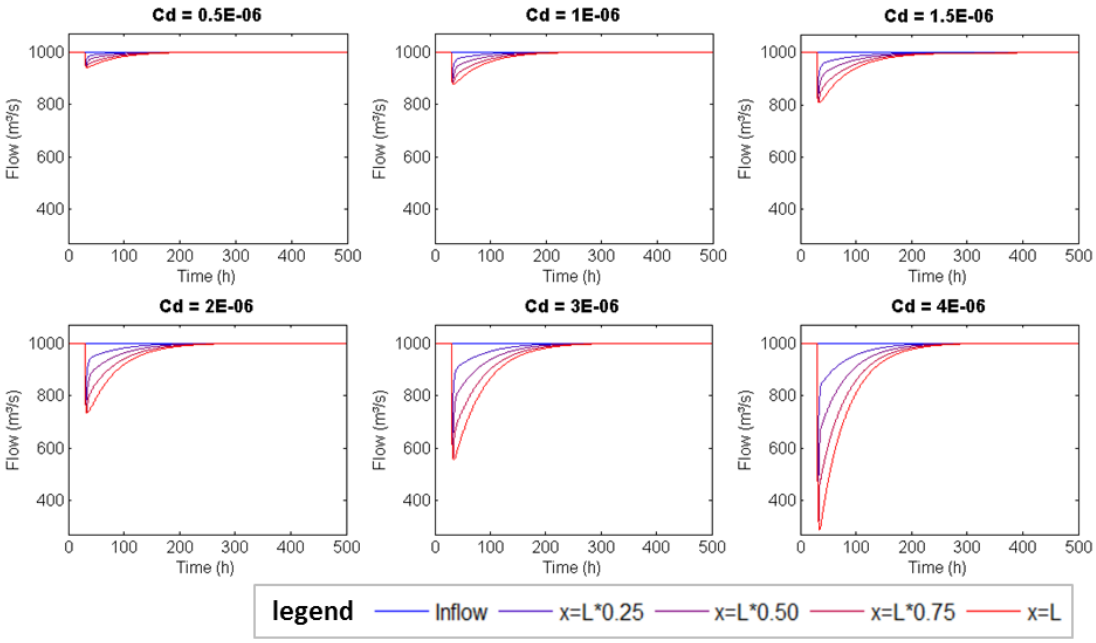

Figure 17 - Flow hydrographs under continuous wind influence for different CD values and U=-10 m/s.

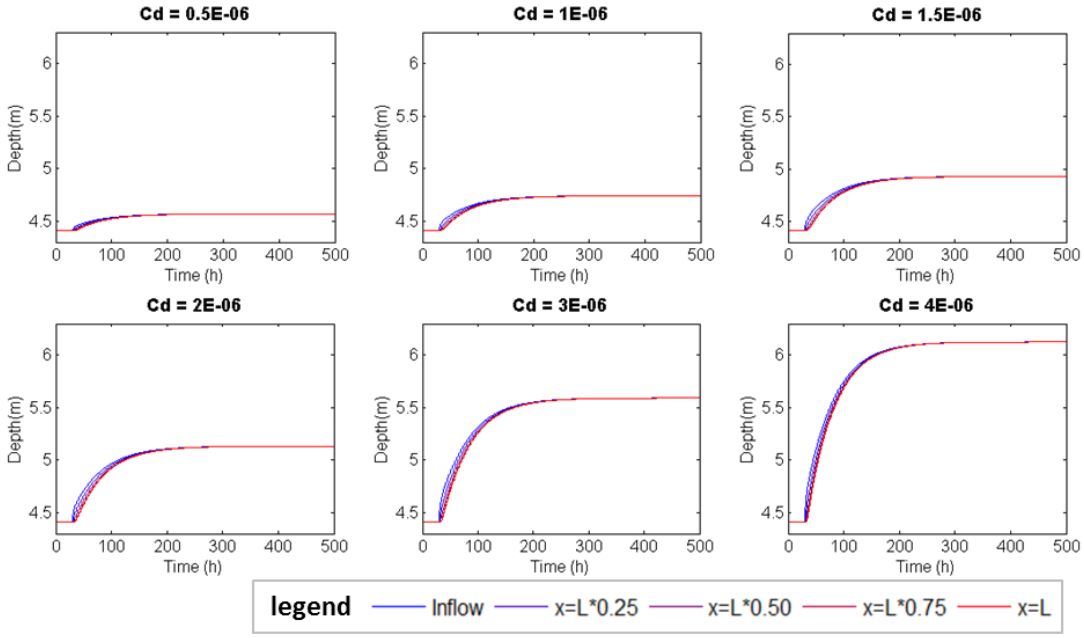

Figure 18 - Water depth versus time Flow under continuous wind influence for different CD values and U=-10 m/s.

This simulation was performed to provide insight over the influence of C_D values on the effect that wind exerts over the flow. It can be seen on figures 18 and 19 that the disturbance cause by wind action is greater for greater C_D values and therefore that this is an important parameter when modelling wind influence over hydrodynamic systems.

Additionally, the influence of C_D values is greater for greater wind velocities. For example, considering a wind velocity of -10m/s, the increase in depth relative variation with a C_D equal to $2x10^{-6}$

compared to using a value of $4x10^{-6}$, was 100%. When a value of wind velocity of -15 m/s was considered, this increase was 167%.

It is important to note that numerical instability was observed for C_D values of $3x10^{-6}$ and $4x10^{-6}$ using wind velocity of -15 m/s, which was corrected by the use of a α value of 0.5. This means that selecting the α value may be necessary to prevent too elevated time-steps and avoid numerical instability, especially under extreme wind velocity conditions.

STAGE 2: MAXIMUM DEPTH VARIATION DUE TO CONTINUOUS WIND INFLUENCE

As a result of simulations performed with the local inertial method with wind influence in hypothetical river flows, new steady state conditions were found after prolonged constant wind action. Considering uniform and permanent flow conditions, under continuous wind action, in the first moments the flow is altered. However, as time passes, the flow converges back to the previous permanent flow value and the alteration due to wind effect is perceived in water depth, which converges to a new value. The resultant depth value is also constant along the channel length.

The observed behavior allowed us to simplify Equation 4 to calculate the maximum variation of depth due to wind influence regarding flows with different pre-established characteristics. The equation was simplified considering 2 main assumptions: (i) in the new equilibrium state the flow is permanent, which means that the flow does not change with time. Therefore, the first term of equation 4 can be neglected; (ii) in the new equilibrium state, the depth does not change with space; hence, the second term of Equation 4 can also be neglected.

Equation 4 can be re-written as:

$$-g.A.S_o + g.A.S_f - B.C_D.|U|.U = 0 \quad (9)$$

Considering that the S_f term can be approximated by the Manning equation and that the channel is rectangular with width much larger than depth, Equation 9 can be re-arranged:

$$h_w = \left(\frac{q.|q|.n^2}{h_w^{7/3}} - \frac{C_D.U.|U|}{g}\right) \cdot \frac{1}{S} \quad (10)$$

Equation 10 must be solved iteratively to calculate h_w, which is the new depth due to continuous wind effect (m). S is the river bottom slope (m/m). q is the flow per unit of width (m^2/s).

The maximum variation of depth due to wind effect can be calculated with equation 11:

$$\frac{dh}{h_o} = \frac{h_w - h_o}{h_o} \times 100 \quad (11)$$

in which h_o is the depth of the permanent uniform flow before wind action calculated with Manning Equation. dh is the maximum depth variation due to continuous wind action (m) and $\frac{dh}{h_o}$ is the percentage variation of depth related to h_o (%).

It is important to highlight that the wind action is constant with no changes in velocity or direction and the flow is uniform with no changes in its characteristics. As the new depth value related to the new steady state achieved after some time, it represents the maximum (minimum) depth that can be achieved due to wind acting against (along) the flow direction.

Abacus of maximum (minimum) depth due to wind acting against (along) the flow direction

The results of applying equations 10 and 11 are displayed as two abacus for values of Manning coefficient of 0.03 (Figure 20) and 0.06 (Figure 21). The maximum percentage variation of water depth due to continuous wind influence is plotted against wind speed (U) displaying several curves related to different flow per unit width (q). The abacus contains 12 plots considering different bed slopes.

An additional figure showing maximum percentage variation of water depth plotted against bed

slope is also presented to better understand the influence of bed slope on the disturbance caused by wind stress (Figure 22).

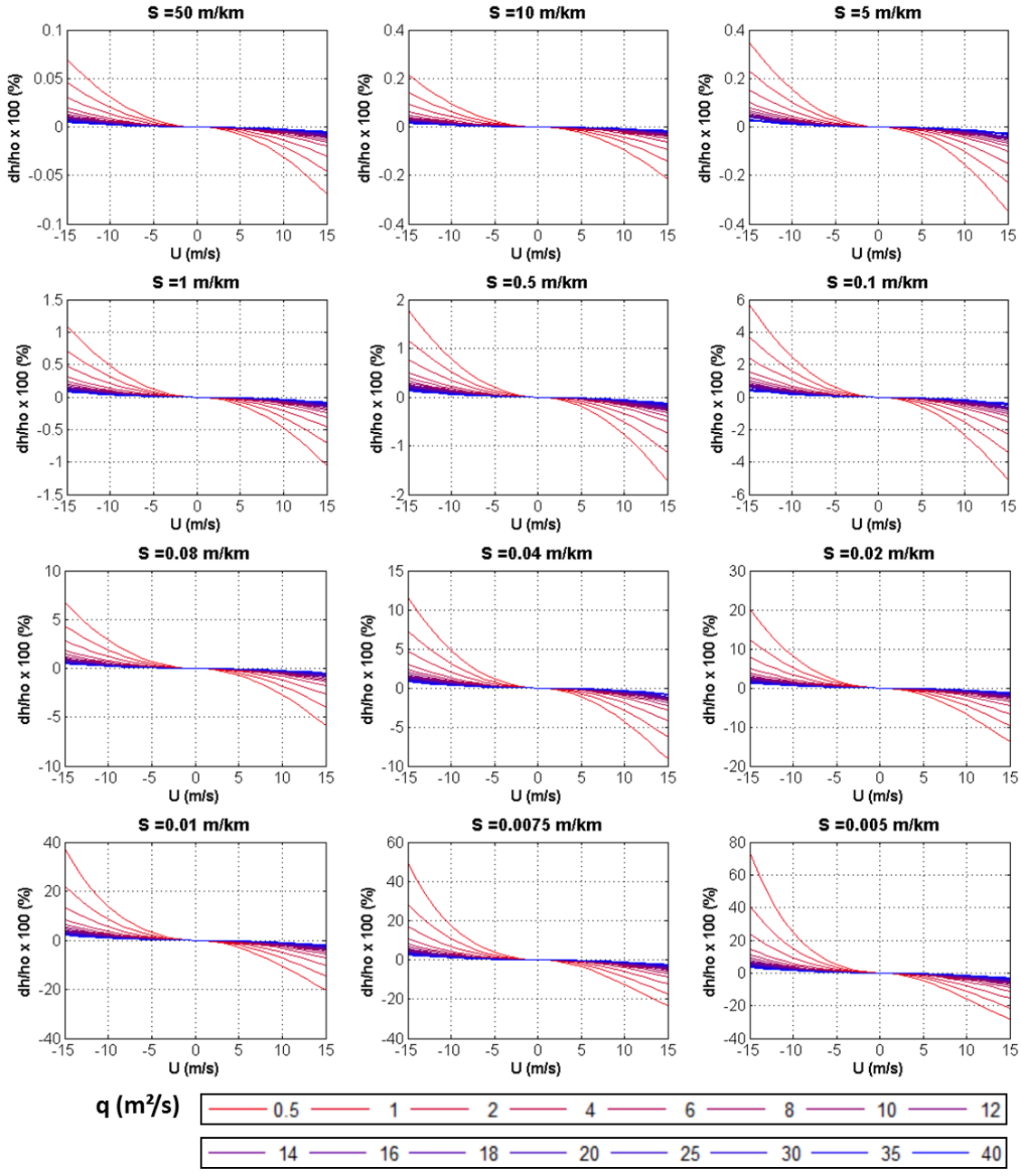

Figure 19 – Abacus that relates percentage depth variation with wind velocity (U) and flow by unit width (q) for different bed slope values (S) considering a Manning coefficient of 0.03.

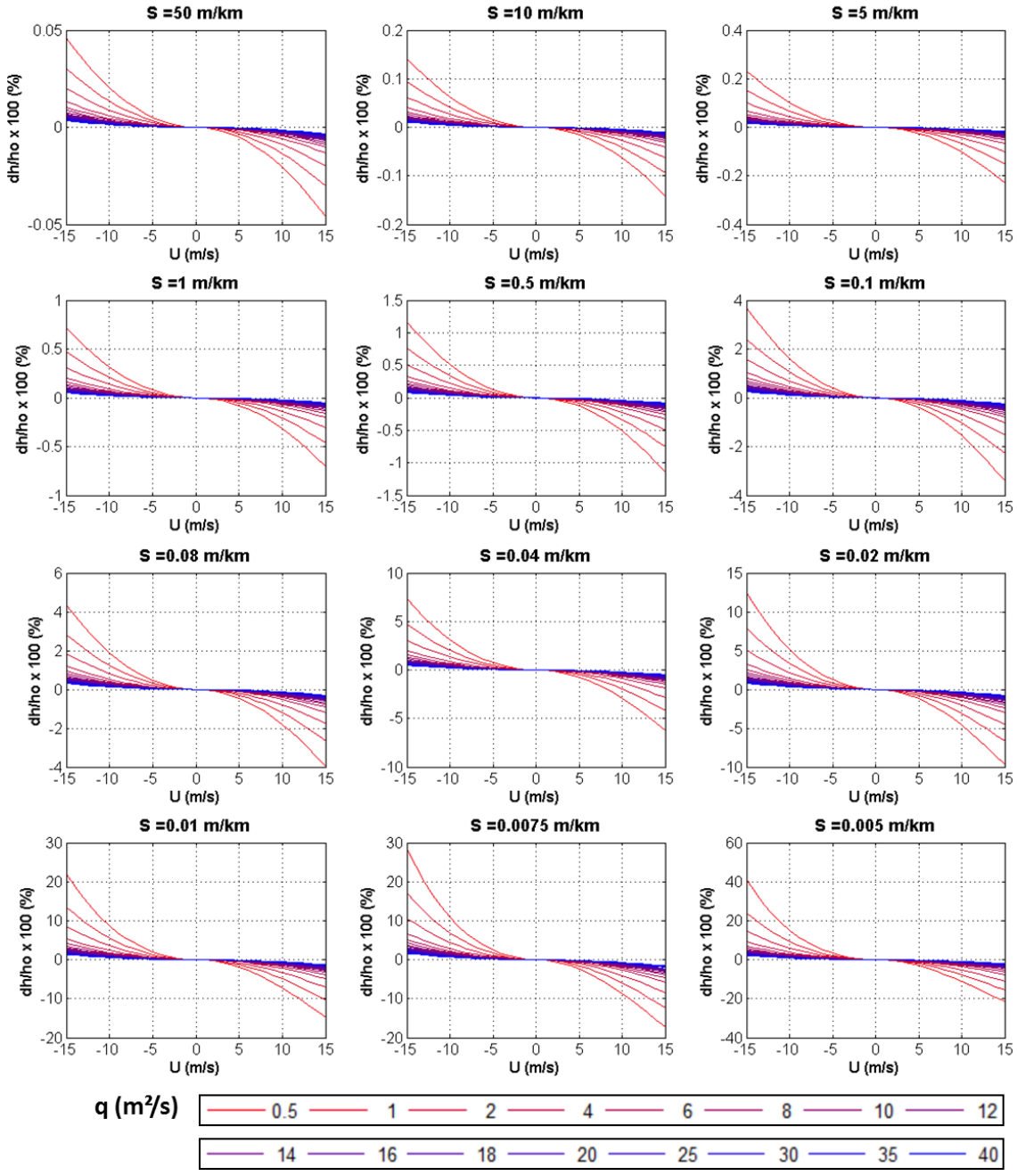

Figure 20 - Abacus that relates percentage depth variation with wind velocity (U) and flow by unit width (q) for different bed slope values (S) considering a Manning coefficient of 0.06.

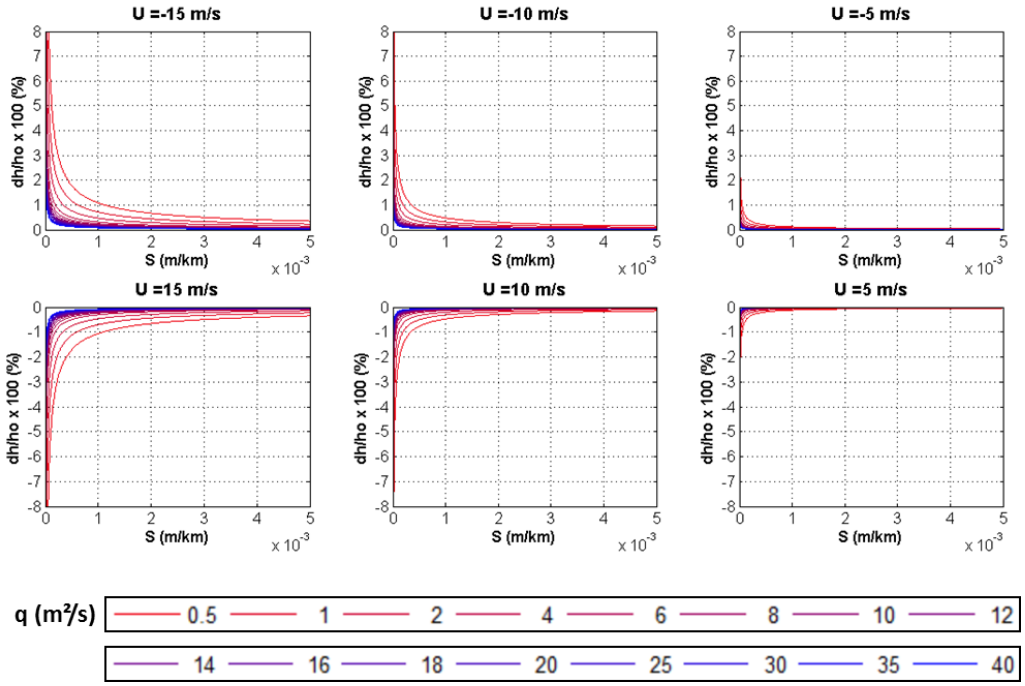

Figure 21 – Relationship between percentage depth variation and bed slope values (S), with curves representing different flow by unit width (q) values and plots for different wind velocities (U) considering a Manning coefficient of 0.03.

The analysis of figures 20, 21 and 22 provided some insights. The first one is that the greater is the value of flow per unit width, the lower is the maximum percentage variation of water depth associate with continuous wind stress. Hence, considering a river that presents similar values of with under high and low flow conditions, this means that percentage variations of depth due to wind action are greater in low flow conditions.

As observed in the simulations, percentage variations of depth are greater when wind blows against the flow direction. This difference of percentage variations when comparing positive and negative wind velocities is more pronounced for higher disturbances in flow due to wind action.

As observed in the simulations, greater percentage depth variations are achieved with lower bed slopes. Figure 22 aids the understanding of how this occurs. Considering slopes steeper than 1m/km, alterations of water depth due to wind action are minimal and don't vary expressively with different values of slope (under this threshold). However, for mild slopes, variations of slope values cause expressive differences of percentage variations of water depth; and when the bed slope tends to zero, the percentage depth variation due to wind action tend to infinite values.

CONCLUSIONS

This study had the objective to evaluate the wind effect in 1d hydrodynamic simulations, based in the local inertial method.

At first glance, it was possible to include wind influence in the algorithm of the inertial flow routing method and obtain a stable solution. The simulations provided results that aided the definition of an equation to predict maximum wind influence in river water depths depending on the river flow characteristics and wind velocities.

From the results it was possible to conclude that:

• Continuous wind action causes an immediate disturbance in 1D water flow which gradually returns to the previous flow value, achieving new permanent state of equilibrium with a different water depth. For negative (positive) wind velocities, which act against (along) the flow direction, the disturbance in flow in negative (positive) causing an increase (decrease) in water depth.

• A pulse of wind action causes a peak in depth values if the wind velocity is negative and a minimum value in case the wind velocity is positive. Water flow presents both greater and lower values than the inflow. This happens because the system was subjected to a temporary forcing and must achieve a state of permanent equilibrium.

• Greater values of Manning coefficient, flow per unit width, and bed slopes cause lower variations of water depth due to wind influence, as greater values of the wind friction coefficient cause the opposite result.

• Small oscillations in flow were perceived due to the interaction with the boundary conditions. These oscillations are favored by the combination of the effects of greater flow celerity and greater magnitude of the disturbance caused by the wind stress. Considering conditions that decrease celerity and/or decrease the disturbance caused by wind action or using a longer river reach may dampen these oscillations.

• Values of the parameter α must be carefully chosen to prevent numerical instability, which can happen more easily under extreme wind velocity conditions.

• The greater the disturbance caused by the wind effect, the greater the time that the system takes to achieve the new permanent flow condition under continuous wind action. Considering the pulse profile, greater disturbances take more time to be dissipated. The same behavior occurs for longer reaches, which shows the greater inertia of large hydrodynamic systems.

• The equation and the abacus proposed can be useful in engineering applications to estimate the maximum wind effect over water levels on a specific river. Therefore, the abacus can aid to define if a river is likely to be influenced by the wind and if this factor should be accounted for.

From these results, next steps of study will be the implementation and testing of the inertial solution considering the wind shear effects in a hydrologic-hydrodynamic model, for discharge simulation and flood forecasting considering this aspect.

REFERENCES

BACOPOULOS, P., HAGEN, S. C., COX, A. T., DALLY, W. R., & BRATOS, S. M. (2012). Observation and simulation of winds and hydrodynamics in St. Johns and Nassau Rivers. Journal of Hydrology, V. 420–421, p. 391–402.

BATES, P. D., HORRITT, M. S., & FEWTRELL, T. J. (2010). A simple inertial formulation of the shallow water equations for efficient two-dimensional flood inundation modelling. Journal of Hydrology, V. 387, p. 33–45.

BLUMBERG, A. F., & MELLOR, G. L. (1987). A Description of a three-dimensional coastal ocean circulation model. In: C.N.K. Mooers (Ed.), Three-dimensional Coastal Ocean Models. Coastal and Estuarine Sciences, V. 4, p. 1-16.

BORCHE, A. (1996). IPH-A: Aplicativo para modelação de estuários e lagoas – Manual de Utilização do sistema. Publicação em Recursos Hídricos Nº 33. IPH/UFRGS, 38 p.

CHANSON, H. (2004). The Hydraulics of Open Channel Flow: An Introduction. Oxford, UK: Butterworth-Heinemann, 2nd edition.

CHOW, V. T., MAIDMENT, D. R., & MAYS, L. W. (1988). Applied Hydrology. McGraw Hill.

COLLISCHONN, W., ALLASIA, D. G., SILVA, B. C., & TUCCI, C. E. (2007). The MGB-IPH model for large-scale rainfall-runoff modelling. Hydrological Sciences Journal, V. 52, p. 878-895.

CUNGE, J. A. (1969). On the Subject of a Flood Propagation Computation Method (Munkingum Method). Journal of Hydraulic Research, V. 7, p. 205-230.

CUNGE, J. A., HOLLY, F. M., & VERWEY, A. (1980). Practical Aspects Computational River Hydraulics. London: Pitman Publishing.

D'AQUINO, C. A., FRANKLIN DA SILVA, L., COUCEIRO, M. A., & PEREIRA, M. D. (2011). Transporte de Sal e Hidrodinâmica do Estuário do Rio Tubarão — SC, Brasil. RBRH — Revista Brasileira de Recursos Hídricos, V. 16, n.3, p. 113-125.

DECHARME, B., DOUVILLE, H., PRIGENT, C., PAPA, F., & AIRES, F. (2008). A new river flooding scheme for global climate applications: off-line evaluation over South America. J. Geophys. Res., V. 113.

DELTARES. (2014). Delft3D-FLOW - Simulation of multi-dimensional hydrodynamic flows and transport phenomena, including sediments- User Manual. Version: 3.15.34158. Delft, The Netherlands.

DHI. (2011). MIKE 21 & MIKE 3 Flow Models - hydrodynamic and Transport Module: Scientific Documentation. http://www.mikebydhi.com.

ESCOBAR, G., VARGAS, W., & BISCHOFF, S. (2004). Wind tides in the Rio de la Plata estuary:

meteorological conditions. Int. J. Climatol., V. 24, p. 1159–1169.

FAN, F. M., PONTES, P. R., PAIVA, R. C., & COLLISCHONN, W. (2014). Avaliação de um método de propagação de cheias em rios com aproximação inercial das equações de Saint-Venant. RBRH - Revista Brasileira de Recursos Hídricos. Volume 19, n. 4, 137-147.

FRAGOSO JR., C. R., NES, E. V., JENSE, J. H., & MARQUES, D. M. (2009). IPH-TRIM3D-PCLake: A three-dimensional complex dynamic model. Environmental Modelling & Software, V. 24(11), p. 1347–1348.

GONG, W., SHEN, J., & HONG, B. (2009). The influence of wind on the water age in the tidal Rappahannock River. Marine Environmental Research, V. 68, p. 203–216.

HATTERMANN, F. F., WATTENBACH, M., KRYSANOVA, V., & WECHSUNG, F. (2005). Runoff simulations on the macroscale with the ecohydrological model SWIM in the Elbe catchmentevalidation and uncertainty analysis. Hydrol. Process. , V. 19 (3), p. 693-714.

HODGES, B. R. (2013). Challenges in Continental River Dynamics. Environmental Modelling & Software, V. 50, p. 16-20.

JI, Z. G. (2008). Hydrodynamics and Water Quality: Modeling Rivers, Lakes and Estuaries. Hoboken, New Jersey: John Wiley & Sons, Inc.

LOPES, V. A. (2015). Modelagem hidrológica integrada da bacia hidrográfica da Laguna dos Patos e seus complexos lagunares usando o modelo MGB-IPH com propagação inercial de vazões. Porto Alegre: Monografia. Universidade Federal do Rio Grande do Sul (UFRGS). Departamento de Engenharia.

LOPES, V. A. (2017). Modelagem hidrológica e hidrodinâmica integrada de bacias e sistemas lagunares com influência do vento. 2017. Dissertação (Mestrado em Recursos Hídricos e Saneamento Ambiental) - Universidade Federal do Rio Grande do Sul, Conselho Nacional de Desenvolvimento Científico e Tecnológico.

MASHRIQUI, H. S., S, H. J., & M, R. (2014). A 1D River Hydraulic Model for Operational Flood Forecasting in the Tidal 3 Potomac: Evaluation for Freshwater, Tidal, and Wind Driven Events. Journal of Hydraulic Engineering Vol. 140 Nº4.

MCCARTHY, G. T. (1938). The unit hydrograph and flood routing. Conference of North Atlantic Division, US Army Corpsof Engineers. New London: CT. US Engineering.

MONTERO, R. A., SCHWANENBERG, D., HATZ, M., & BRINKMANN, M. (2013). Simplified hydraulic modelling in model predictive control of flood mitigation measures along rivers. Journal of Applied Water Engineering and Research, V. 1, p. 17-27.

NEITSCH, S. L., ARNOLD, J. G., KINIRY, J. R., WILLIAMS, J. R., & KING, K. W. (2002). Soil and water assessment tool - theorical documentation, version 2000. Temple, Grassland, Soil and Eater Research Laboratory - Agricultural Research Service (p. 212 p.). Blackland Research Center – Texas Agricultural Experiment Station.

NGO-DUC, T., LAVAL, K., RAMILLIEN, G., & POLCHER, J. (2007). Validation of the land water storage simulated by ORCHIDEE with GRACE data: role of the routing scheme. Water Resources Research, 43(4):W04427, doi:10.1029/2006WR004941.

PAZ, A. R., REIS, L. G., & LIMA, H. V. (2005). Uso de modelagem hidrodinâmica visando a segmentação de corpos d'água rasos para enquadramento: o caso do Lago Guaíba (RS). In: XVI Anais do Simpósio Brasileiro de Recursos Hídricos. João Pessoa, 20 a 24 de novembro de 2005.

PONTES, P. R., COLLISCHONN, W., FAN, F. M., PAIVA, R. C., & BUARQUE, D. C. (2015). Modelagem Hidrológica e Hidráulica de Grande Escala com Propagação Inercial de Vazões. RBRH - Revista Brasileira de Recursos Hídricos.

PONTES, P. R., FAN, F. M., FLEISCHMANN, A. S., PAIVA, R. C., BUARQUE, D. C., SIQUEIRA, V. A., et al. (2017). MGB-IPH model for hydrological and hydraulic simulation of large

floodplain river systems coupled with open source GIS. Environmental Modelling & Software, V. 94, p. 1-20.

RAMÓN, C. L., PRATS, J., & RUEDA, F. J. (2016). The influence of flow inertia, buoyancy, wind, and flow unsteadiness on mixing at the asymmetrical confluence of two large rivers. Journal of Hydrology, V. 539, p. 11–26.

USACE. (2010). HEC-RAS River Analysis System: Hydraulic Reference Manual Ver. 4.1. 609 Second Street, Davis, CA 95616: U.S. Army Corps of Engineers, Hydrologic Engineering Center.

WU, J. (1982). Wind-stress coefficients over sea surface from breeze to hurricane. J. Geophys. Res., V. 87, C12, p. 9704─9706.

YAMAZAKI, D., DE ALMEIDA, G. A., & BATES, P. D. (2013). Improving computational efficiency in global river models by implementing the local inertial flow equation and a vector-based river network map. Water Resources Research, V. 49(11), p. 7221-7235.